Hydrol. Earth Syst. Sci. Discuss., 3, 2437–2471, 2006
www.hydrol-earth-syst-sci-discuss.net/3/2437/2006/

Hydrology and Earth System Sciences Discussions

Papers published in *Hydrology and Earth System Sciences Discussions* are under open-access review for the journal *Hydrology and Earth System Sciences*

A parameter identifiability study of two chalk tracer tests

S. A. Mathias[1], **A. P. Butler**[1], **T. C. Atkinson** [2,3], **S. Kachi**[3,*], **and R. S. Ward**[3,**]

[1]Department of Civil and Environmental Engineering, Imperial College London, London SW7 2AZ, UK
[2]Department of Earth Sciences, University College London, London WC1E 6BT, UK
[3]School of Environmental Sciences, University of East Anglia, Norwich NR4 7TU, UK
[*]now at: Institut des Sciences de la Terre, I.N.E.S. de Tebessa, Tebessa 1200, Algeria
[**]now at: Environment Agency, Solihull B29 7HX, UK

Received: 2 June 2006 – Accepted: 15 July 2006 – Published: 29 August 2006

Correspondence to: S. A. Mathias (simon.mathias@imperial.ac.uk)

Abstract

As with most fractured rock formations, Chalk is highly heterogeneous. Therefore, meaningful estimates of model parameters must be obtained at a scale comparable with the process of concern. These are frequently obtained by calibrating an appropriate model to observed concentration-time data from radially convergent tracer tests (RCTT). Arguably, an appropriate model should consider radially convergent dispersion (RCD) and Fickian matrix diffusion. Such a model requires the estimation of at least four parameters. A question arises as to whether or not this level of model complexity is supported by the information contained within the calibration data. Generally modellers have not answered this question due to the calibration techniques employed. A dual-porosity model with RCD was calibrated to two tracer test datasets from different UK Chalk aquifers. A multivariate sensitivity analysis, which assumed only a priori upper and lower bounds for each model parameter, was undertaken. Rather than looking at measures of uncertainty, the shape of the multivariate objective function surface was used to determine whether a parameter was identifiable. Non-identifiable parameters were then removed and the procedure was repeated until all remaining parameters were identifiable.

It was found that the single fracture model (SFM) (which ignores mechanical dispersion) obtained the best mass recovery, excellent model performance and best parameter identifiability in both the tests studied. However, there was no objective evidence suggesting that mechanical dispersion was negligible. Moreover, the SFM (with just two parameters) was found to be good at approximating the Single Fracture Dispersion Model SFDM (with three parameters) when different, and potentially erroneous parameters, were used. Overall, this study emphasises the importance of adequate temporal sampling of breakthrough curve data prior to peak concentrations, to ensure adequate characterisation of mechanical dispersion processes, and continued monitoring afterwards, to ensure adequate characterisation of fracture spacing (where possible), when parameterising dual-porosity solute transport models.

1 Introduction

Chalk aquifers represent around 20% of UK water supplies. To help protect these important aquifers from contamination we need appropriate solute transport models. The Chalk is a dual-porosity medium with a fracture porosity of around 1% and a matrix porosity of between 25% and 35% (Price et al., 1993). While the fracture porosity is highly permeable, the matrix porosity is not. Consequently flow predominately occurs in the fractures whilst water stored in the matrix is largely immobile. Solute transport in such a medium is controlled by at least three processes: advection, mechanical dispersion and diffusive exchange between moving water in the fractures and immobile water in the matrix (Barker, 1993). Therefore, an appropriate solute transport model requires parameters such as dispersivities, porosities, diffusion coefficients and fracture spacings.

The Chalk, as with most fractured rock formations, is highly heterogenous. Therefore, meaningful estimates of the desired model parameters must be obtained at a scale comparable with the modelling process of concern. Consequently, these parameters are frequently obtained from radially convergent tracer tests (e.g. Kachi, 1987; Ward, 1989, 1996; Atkinson et al., 2000).

Radially convergent tracer tests involve pumping an abstraction well to obtain a quasi-steady radially convergent flow-field. A tracer is then injected in a neighbouring borehole which lies within the radially convergent flow-field. Tracer concentrations are then monitored and recorded at the abstraction well. An appropriate mathematical model can then be calibrated to the observed concentration-time data (breakthrough curve) to obtain the desired parameters.

Arguably, an appropriate model should consider radially convergent dispersion and Fickian matrix diffusion. An example is proposed by Moench (1995). Such a model requires the estimation of at least four parameters (see Sect. 3). A question arises as to whether or not this level of structural complexity in the model is supported by the information contained within the data used for calibration (Beven and Binley, 1992).

HESSD
3, 2437–2471, 2006

Generally modellers have not addressed this question because they have not used a formal methodology to investigate parameter identifiability.

Subsurface tracer test models are often calibrated by manual-graphical fitting to observed data (e.g. Moench, 1995; Atkinson et al., 2000; Becker and Shapiro, 2000). More recently, McKenna et al. (2001) used a parameter estimation scheme that minimised the squared residuals between the observed and modelled data. Parameter identifiability was then quantified by using the normalised Jacobian matrix around the least squares solution. As opposed to this local sensitivity analysis, we perform a regionalised sensitivity analysis, where the response surface of a model performance over a parameter space (specified a priori) is analysed. Instead of looking at quantified measures of identifiability for each of the parameters (as with McKenna et al., 2001) a decision is made as to whether a parameter is identifiable or not. If a parameter is found to be non-identifiable, it is further assumed that the physical process represented by that parameter is not relevant in this case. The process is then removed from the model formulation and a new, more simplified model is recalibrated. This procedure is repeated until all parameters are found to be identifiable.

Monte Carlo simulation is used (in a similar way to Wagener et al., 2001; Mcintyre et al., 2002; Sincock et al., 2003; Smith and Wheater, 2004) as follows: 100 000 Parameter sets are selected from log-uniform random distributions between a priori upper and lower bound estimates. The models are run for each of the parameter sets. The model performance of each model with the observed tracer breakthrough data is measured using the root mean squared error RMSE:

$$\mathrm{RMSE} = \sqrt{\frac{1}{N}\sum_{n=1}^{N}(c_{e,n} - c_{o,n})^2} \quad (1)$$

where $c_{e,n}$ and $c_{o,n}$ are modelled and observed tracer concentrations at the abstraction well respectively and N is the number of data points.

The parameter set with the lowest RMSE is assumed to be the best estimate of the "true" values for the field situation of the experiment, subject to the assumptions that all

the processes in the current model were actually important in generating the observed breakthrough curve. Parameter identifiability is then explored by studying 'dotty' plots of parameter values against log(RMSE). Parameters with dotty plots that show structural convergence to the minimum RMSE are deemed identifiable. Parameters which do not are deemed non-identifiable.

2 The tracer tests

For the analysis, two previous radially convergent tracer tests in Chalk aquifers were chosen. Specifically we studied the Horseheath (Kachi, 1987) and South Farm (Ward, 1989) tracer tests (Figs. 1 and 2 show the BTCs). Details of the tests are summarised in Table 1. Further information is also given by Ward et al. (1998, Sites No. 8 and 46).

Note that similar model comparison studies using the South Farm data have already been reported by Atkinson et al. (2000, 2001). However, the different models were only compared in terms of parameter values, mass recovery and visual fitting. Here we are also looking at parameter identifiability.

3 The tracer test models

Following Barker (1982) we make the following assumptions which are common to all the models considered here: Identical slabs of matrix material are separated by equally spaced, planar fractures. The matrix is homogenous and saturated with immobile water. Solute transfer between the fractures and matrix and within the matrix occurs by molecular diffusion in the immobile water in a direction perpendicular to the plane of the fractures. There is no concentration gradient across the fractures.

Following Barker et al. (2000), it is useful to introduce an advective travel time, t_a, a characteristic fracture diffusion time, t_{cf}, and a characteristic matrix block diffusion

time, t_{cb}:

$$t_a = \frac{\pi R^2 h \phi_f}{Q}, \quad t_{cf} = \frac{(a/\phi_m)^2}{D_A}, \quad t_{cb} = \frac{b^2}{D_A} \tag{2}$$

where R is the distance between the pumping well and the injection well, h is the aquifer thickness, ϕ_f is the fracture porosity, Q is the abstraction rate, a is the fracture half-width, ϕ_m is the matrix porosity, D_A is the apparent diffusion coefficient of the tracer in the matrix and b is the matrix block half-width. The various dimensions of the model domain are further summarised in Fig. 3.

It is also useful to introduce the following dimensionless transformations:

$$P = \frac{R}{\alpha_L}, \quad r_D = \frac{r}{R}, \quad x_D = \frac{x}{b} \tag{3}$$

where α_L is the dispersivity (whereby the mechanical dispersion coefficient for the fracture domain is assumed to be found from $D_L = \alpha_L |v|$ and v is a fracture-water velocity). P is often referred to as the Peclet number.

Following Moench (1995), solute concentrations in the fractures, c_f can then be described by

$$\frac{\partial C_f}{\partial t} - \frac{1}{t_a r_D}\left(\frac{\partial C_f}{\partial r_D} + \frac{1}{P}\frac{\partial^2 C_f}{\partial r_D^2}\right) - \frac{1}{(t_{cf} t_{cb})^{1/2}}\frac{\partial C_m}{\partial x_D}\bigg|_{x_D=1} = 0 \tag{4}$$

subjected to the initial and boundary conditions:

$$\begin{aligned} C_f &= 0, && r_D \geq 0, t = 0 \\ \frac{\partial C_f}{\partial r_D} &= 0, && r_D = 0, t > 0 \\ C_f + \frac{1}{P}\frac{\partial C_f}{\partial r_D} &= \delta(t), && r_D = 1, t > 0 \end{aligned} \tag{5}$$

where t is time after the tracer injection, $C_f=(Q/M)c_f$ is the normalised solute concentration in the fractures, M is the total mass of tracer injected in the modelled system and $\delta(t)$ denotes the Dirac delta function, which implies that the tracer injection occurs instantaneously. Also note that both the radii of the injection and abstraction wells are assumed infinitesimally small (Moench, 1995, offers ways of relaxing this assumption but it introduces further parameter requirement).

The boundary conditions in Eq. (5) are often referred to as the Danckwerts (1953) conditions. For further physical explanation the reader is referred to Schwartz et al. (1999).

Solute concentrations in the matrix, c_m are governed by (e.g. Barker, 1982, 1985)

$$\frac{\partial C_m}{\partial t} - \frac{1}{t_{cb}} \frac{\partial^2 C_m}{\partial x_D^2} = 0 \tag{6}$$

subjected to the initial and boundary conditions:

$$\begin{aligned} &C_m = 0, \quad x_D \geq 0, r_D \geq 0, t = 0 \\ &\frac{\partial C_m}{\partial x_D} = 0, x_D = 0, r_D \geq 0, t > 0 \\ &C_m = C_f, \quad x_D = 1, r_D \geq 0, t > 0 \end{aligned} \tag{7}$$

where $C_m=(Q/M)c_m$ is the normalised solute concentration in the matrix.

The solute concentration in the abstraction well, c_e can then be found from

$$c_e(t) = c_f(r_D = 0, t) \tag{8}$$

Note that $C_e=(Q/M)c_e$ denotes the normalised concentration in the abstraction well.

By applying the Laplace transform

$$\hat{C}(p) = \int_0^\infty C(t)e^{-pt}dt \tag{9}$$

following Moench (1989, 1995), the Laplace transform solution for the modelled abstraction concentration is obtained

$$\hat{C}_e(p) \equiv \hat{C}_f(r_D = 0, p) = e^{P/2} G(p) \tag{10}$$

where:

$$\begin{aligned} G(p) = {} & [A'_0 B_0 - A_0 B'_0][\sigma^{1/3}(A'_0 B'_1 - A'_1 B'_0) \\ & + 0.5(A'_1 B_0 - A_0 B'_1) + 0.5(A'_0 B_1 - A_1 B'_0) \\ & + 0.25\sigma^{-1/3}(A_1 B_0 - A_0 B_1)]^{-1} \end{aligned} \tag{11}$$

$$\begin{aligned} A_0 &= \mathrm{Ai}(\sigma^{1/3} y_0), \quad B_0 = \mathrm{Bi}(\sigma^{1/3} y_0) \\ A'_0 &= \mathrm{Ai}'(\sigma^{1/3} y_0), \quad B'_0 = \mathrm{Bi}'(\sigma^{1/3} y_0) \\ A_1 &= \mathrm{Ai}(\sigma^{1/3} y_1), \quad B_0 = \mathrm{Bi}(\sigma^{1/3} y_1) \\ A'_1 &= \mathrm{Ai}'(\sigma^{1/3} y_1), \quad B'_0 = \mathrm{Bi}'(\sigma^{1/3} y_1) \end{aligned} \tag{12}$$

$$\sigma = \frac{2 t_a \lambda(p)}{P^2}, \quad y_0 = \frac{1}{4\sigma}, \quad y_1 = P + \frac{1}{4\sigma} \tag{13}$$

$$\lambda(p) = p + p \left(\frac{t_{cb}}{t_{cf}} \right)^{1/2} F[(t_{cb} p)^{1/2}] \tag{14}$$

$$F(\xi) = \xi^{-1} \tanh(\xi), \quad \xi = (t_{cb} p)^{1/2} \tag{15}$$

and Ai and Bi are Airy functions. The above solution can be evaluated using a numerical inverse Laplace transform. We use our own MATLAB implementation of the de Hoog et al. (1982) algorithm.

Note that $F(\xi)$ is often referred to as the block-geometry function for a slab-matrix (Barker, 1985, 1988; Carrera et al., 1998; Barker et al., 2000; Fretwell et al., 2005;

Mathias et al., 2005). (A more generalised expression of the block-geometry function is (Barker, 1988; Barker et al., 2000)

$$F(\xi, \nu) = \xi^{-1} I_{\nu/2}(\nu\xi)/I_{\nu/2-1}(\nu\xi) \tag{16}$$

where ν is a non-integer number of dimensions of a ν-dimensional rotationally symmetric matrix block, I_ν is an ν-order modified Bessel function of the first kind and the matrix block half-width, b now represents the matrix block's volume to surface area ratio. For a slab, ν=1.)

It is useful to consider some limiting cases of Eq. (10):

When the fracture spacing is infinitely large (i.e. $b \to \infty$)

$$\lim_{t_{cb}\to\infty} \lambda(p) = p + (p/t_{cf})^{1/2} \tag{17}$$

When the diffusion coefficient is infinitesimally small (i.e. $D_A \to 0$)

$$\lim_{t_{cf}\to\infty} \lambda(p) = p \tag{18}$$

When the dispersivity is very small as compared to the distance being considered (i.e. $\alpha_L << R$) (e.g. Barker, 1982)

$$\lim_{P\to\infty} \hat{C}_e(p) = \exp[-t_a \lambda(p)] \tag{19}$$

When the fracture spacing is infinitely large and the dispersivity is very small as compared to the distance being considered (Maloszewski and Zuber, 1985)

$$C_e(t) = \left[\frac{t_a^2}{4\pi t_{cf}(t-t_a)^3}\right]^{1/2} \exp\left[-\frac{t_a^2}{4t_{cf}(t-t_a)}\right] \tag{20}$$

for $t > t_a$.

In this study we employ five related models:

a) Parallel fracture dispersion model (PFDM), $C_e(t, t_a, t_{cf}, t_{cb}, P)$;
b) Single fracture dispersion model (SFDM), $C_e(t, t_a, t_{cf}, \infty, P)$;
c) Dispersion model (DM), $C_e(t, t_a, \infty, \infty, P)$;
d) Parallel fracture model (PFM), $C_e(t, t_a, t_{cf}, t_{cb}, \infty)$;
e) Single fracture model (PFDM), $C_e(t, t_a, t_{cf}, \infty, \infty)$.

4 On mass recovery

There are different possible approaches to adopting a value for the parameter M (the total mass of tracer injected into the modelled system). For example it could be set equal to the mass that was actually injected, M_{inj}. However, in practice there are often difficulties in obtaining a realistic fit of the model to the data when this is done. Our approach is to constrain M by setting the mass recovered from the borehole during the monitoring time of the tracer test to be equal in both the modelled and real systems. This requires that

$$\text{trapz}(t_n, c_{\text{obs},n}) = \text{trapz}(t_n, c_{e,n}), \quad n = 1 \ldots N \tag{21}$$

where $c_e = (M/Q)C_e$ and trapz denotes an integral using the trapezoidal method.

It follows that a value of M can be calculated for each model (and parameter set) from

$$M = Q \frac{\text{trapz}(t_n, c_{\text{obs},n})}{\text{trapz}(t_n, C_{e,n})}, \quad n = 1 \ldots N \tag{22}$$

An advantage of doing this is that the model's mass recovery, $M/M_{inj} \times 100\%$ can be used as a model performance measure in addition to the RMSE.

5 Results

Figure 4 shows the dotty plots for the Horseheath tracer test. With the PFDM, both t_a and t_{cf} appear to be identifiable. In contrast the rough lower surface of the t_{cb} dotty plot indicates that model performance (i.e. the RMSE) is insensitive to its value. The P dotty plot suggests that model performance increases with increasing P but once $P>10$, model performance becomes much less sensitive to P as well.

With the SFDM it is assumed $t_{cb} \rightarrow \infty$ and it is apparent that there is very little loss in model performance (see Table 2). With the DM it is assumed that $t_{cf} \rightarrow \infty$ such that we are essentially modelling a single porous medium. As a result the optimum advective travel time is increased by an order of magnitude and the Peclet number becomes very small. Also note from Table 2 that the DM has the worst model performance and mass recovery.

With the PFM and the SFM, longitudinal dispersion is assumed negligible (i.e. $P \rightarrow \infty$) with only a minor reduction in model performance compared to the PFDM and SFDM. Again, t_{cb} appears to be non-identifiable. It seems that the only parameters we can have any confidence in are t_a and t_{cf}. Interestingly almost exactly the same conclusions may be drawn from the South Farm tracer test (see Figs. 2 and 5 along with Table 3).

6 On the feasibility of measuring t_{cb}

Haggerty et al. (2000) showed that for large times, (i.e. $t>>t_a$)

$$C_e(t) = \frac{2t_a}{t_{cb}^{3/2} t_{cf}^{1/2}} \sum_{n=0}^{\infty} A_n \exp(-A_n t/t_{cb}) \tag{23}$$

where $A_n=(2n+1)^2\pi^2/4$.

When $t_{cb}\rightarrow\infty$ Eq. (23) reduces further to (Haggerty et al., 2000)

$$\lim_{t_{cb}\rightarrow\infty} C_e(t) = \left[\frac{t_a^2}{4\pi t_{cf}}\right]^{1/2} t^{-3/2} \tag{24}$$

Figure 6 shows plots of Eqs. (23) and (24). It can be seen that the PFM only starts to deviate from the SFM once $t>t_{cb}/10$. Moreover, taking into account the error one might expect with measuring tracer concentrations at these later times, it could be argued that the PFM cannot be distinguished from the SFM whilst $t\leq t_{cb}$.

From Fig. 6, it can be concluded that it is only possible to estimate t_{cb} from a tracer test when the time for which measurable tracer concentrations are sustained at the measurement point is greater than t_{cb}. Table 4 shows some calculated fracture spacings for a range of apparent diffusion coefficients and characteristic block diffusion times.

Fracture spacings in Chalk aquifers typically range between around 0.05 and 2.0 m (Bloomfield, 1996). The Horseheath and South Farm tracer tests lasted for 170 and 500 h respectively. Table 4 indicates that even for a test that lasted 1000 h, the largest fracture spacing detectable would have been 0.038 m which is below the lower bound of the Bloomfield range. It is therefore no surprise that the t_{cb} parameter was found to be non-identifiable (see dotty plots in Figs. 4 and 5). More alarmingly, even if a test lasting 10 000 h (417 days) was performed, the largest detectable fracture spacing would still

be less than 0.12 m. Clearly, forced-gradient tracer tests are completely inappropriate for measuring t_{cb} (also see Barker et al., 2000).

Note that some authors have opted for non-Fickian diffusion mechanisms that assume random distributions of mass-transfer rate (related to random distributions of matrix block sizes) to describe the fracture-matrix solute exchange (Haggerty and Gorelick, 1995; Haggerty et al., 2000, 2001; McKenna et al., 2001). This approach would be inappropriate for interpreting radially convergent tracer tests in Chalk because there would probably not be enough time for the tracer plume to feel the minimum matrix block size, let alone the whole distribution.

7 On the importance of mechanical dispersion

Figures 4 and 5 show that only t_a and t_{cf} are strongly identifiable. Furthermore, Tables 2 and 5 indicate best mass recovery when mechanical dispersion is assumed negligible (i.e. the PFM and SFM) but the improvement on the hybrid models (i.e. PFDM and SFDM) is only moderate. This raises the question as to whether mechanical dispersion is important or not.

Barker et al. (2000) suggest that when $t_a > 3t_{cf}$ and $t_a << t_{cb}$, mechanical dispersion can be neglected. The basis for this is as follows. Dispersivities are normally one-tenth of the distance travelled (i.e. $P=10$). If the "effective dispersivity" caused by the matrix diffusion is greater than the distance travelled (i.e. $P<1$) then the mechanical dispersion should be negligible. According to Barker (1993), "effective dispersivities" were calculated by equating the dilution (the concentration of a constant tracer pulse of duration t_a at the input boundary divided by the peak concentration of its breakthrough curve at a downstream control-point) due to an SFM with that of a uniform advective dispersion model. From Tables 2 and 5 it can be seen that for the SFM, $t_a = 15.1t_{cf}$ at Horseheath and $t_a = 17.8t_{cf}$ at South Farm. On the face of it, Barker's rule could be invoked to support the hypothesis that mechanical dispersion was negligible for the two tests studied.

However, Barker et al. (2000) cited peak concentration as the sole criterion for equivalence between just two models, the DM and the SFM (for a fuller treatment see Wright, 2002). In the more general case considered here, we are interested in reproducing the entire breakthrough curve using DM, SFM and the hybrid SFDM. Figure 7 compares the SFM with the SFDM (with P=10) for a range of t_a/t_{cf} ratios. It can be seen that even when t_a=24t_{cf}, the mechanical dispersion due to P=10 is not negligible. Mechanical dispersion only becomes negligible when the dispersivity is small as compared to the length being considered (i.e. the Peclet number, P becomes large).

The dotty plots in Figs. 4a and b and 5a and b show that model performance became much less sensitive to P for P>10. The optimum estimates of P using the SFDM were 28.2 and 53.6 for Horseheath and South Farm respectively, which suggest relatively small dispersivities. In Fig. 1 it can be seen that the calibrated SFM and SFDM are almost identical apart from the peak value. In Fig. 2 the calibrated SFM and SFDM are visually indistinguishable. However, the optimum estimates of t_a and t_{cf} are substantially different (see Tables 2 and 3). Clearly, there is a parameter trade-off between P, t_a and t_{cf}.

To explore this further, the SFDM was calibrated using a simplex search method available with MATLAB called FMINSEARCH (Lagarias et al., 1998) and fixing P a priori. Note that FMINSEARCH is not suitable for high dimensional problems.

Tables 5 and 6 contain the optimised values for the Horseheath and South Farm tests respectively. It can be seen that the RMSE and mass recovery vary very little for $P \geq 10$, particularly in relation to the noise level in the observed data. Furthermore, the model outputs are virtually indistinguishable (see Figs. 8 and 9) but the range of optimised parameter values in Tables 5 and 6 is substantial.

It seems that mechanical dispersion may have been quite important at these test sites despite the fact that P is not a strongly identifiable parameter (recall Sect. 5). However, the parameter trade-off demonstrated in Tables 5 and 6 shows that the chosen value of P has a profound influence on corresponding values of t_a and t_{cf} at these sites.

Figures 10 and 11 show identical plots to those in Figs. 8 and 9 but on log-log scales. It can be seen that much more data is needed before the time to peak, as it is only here that the models (as detailed in Tables 5 and 6) diverge in a substantial way.

8 Conclusions

A four parameter model was calibrated to radially convergent tracer test data-sets from two Chalk aquifers. Through studies of the multivariate parameter space it was found that the characteristic block diffusion time, t_{cb} was non-identifiable. Although both t_a and P were found to be identifiable using just the advection dispersion model (DM), this model was ruled out on the grounds of poor performance in terms of both RMSE and mass recovery (see Tables 2 and 3). Specifically, the DM was unable to reproduce the long tails seen in the breakthrough curves from both tracer tests (dashed lines in Figs. 1 and 2).

No tracer test data were available for times greater than 500 h after tracer injection. It is therefore not surprising that t_{cb} was non-identifiable, as a fracture spacing of just 4 cm with an apparent diffusion coefficient of 10^{-10} m^2/s would take over 1000 h to detect.

It was found that the single fracture model (SFM) gave the best mass recovery, excellent model performance and best parameter identifiability in both the tests studied. Following the suggestion of Barker et al. (2000) that mechanical dispersion becomes negligible when $t_a > 3t_{cf}$, it might be thought that this was because mechanical dispersion was overshadowed by the effects of matrix diffusion. However, our own analysis has shown that this is not the case (see Fig. 7).

Further analysis showed that because P was weakly identifiable, a large set of correlated values of P, t_a and t_{cf} would lead to equally good model fits. As a special case, the SFM (with just two parameters) was found to be good at approximating the SFDM (with three parameters) when different parameters were used. To resolve this ambiguity, more and better quality data is needed at the very start of the breakthrough

curve, to constrain the mechanical dispersion parameter, P.

Overall, this study emphasises the importance of adequate temporal sampling of breakthrough curve data prior to peak concentrations and continued monitoring afterwards to ensure adequate characterisation of fracture spacing (where possible) when parameterising dual-porosity solute transport models.

Acknowledgements. Funding through the NERC LOCAR research programme (Project numbers NER/T/S/2001/00941 and NER/T/S/2001/00956). R. Ward is also grateful for his NERC training award.

References

Atkinson, T. C., Ward, R. S., and O'Hannelly, E.: A radial-flow tracer test in Chalk: comparison of models and fitted parameters, in: Tracers and Modelling in Hydrogeology, edited by: Dassargues, A., Tracers and Modelling in Hydrogeology (Proceedings of the TraM'2000 conference held at Liège, Belgium, May 2000), IAHS Publ., 262, 7–15, 2000. 2439, 2440, 2441

Atkinson, T. C., Barker, J. A., Ward, R. S., and Low, R. G.: Radon: An indicator of solute transport in double-porosity aquifers, in: New Approaches Chracterizing Groundwater Flow, edited by: Wohnlich, S., 441–445, Swets & Zeitlinger Lisse, 2001. 2441

Barker, J. A.: Laplace Transform Solutions for Solute Transport in Fissured Aquifers, Adv. Water Resour., 5, 98–104, 1982. 2441, 2443, 2445

Barker, J. A.: Block-geometry functions characterising transport in densely fissured media, J. Hydrol., 77, 263–279, 1985. 2443, 2444

Barker, J. A.: A Generalized Radial Flow Model for Hydraulic Tests in Fractured Rock, Water Resour. Res., 24, 1796–1804, 1988. 2444, 2445

Barker, J. A.: Modelling groundwater flow and transport in the Chalk, in: The Hydrogeology of the Chalk of North-West Europe, edited by: Downing, R. A., Price, M. and Jones, G. P., 59–66, Clarendon Press, Oxford, 1993. 2439, 2449

Barker, J. A., Wright, T. E. J., and Fretwell, B. A.: A pulsed-velocity method of double-porosity solute transport modelling, in: Tracers and Modelling in Hydrogeology, edited by Dassargues, A., Tracers and Modelling in Hydrogeology (Proceedings of the TraM'2000 conference held

at Liège, Belgium, May 2000), IAHS Publ., 262, 297–302, 2000. 2441, 2444, 2445, 2449, 2450, 2451
Becker, M. W. and Shapiro, A. M.: Tracer transport in fractured crystalline rock: Evidence of nondiffusive breakthrough tailing, Water Resour. Res., 36, 1677–1686, 2000. 2440
Beven, K. J. and Binley, A. M.: The future of distributed models: model calibration and uncertainty prediction, Hydrol. Process., 6, 279–298, 1992. 2439
Bloomfield, J.: Characterisation of hydrologically sigificant fracture distributions in the Chalk: an example from the Upper Chalk of southern England, J. Hydrol., 184, 355–379, 1996. 2448
Carrera, J., Sanchez-Vila, X., Benet, I., Medina, A., Galarza, G., and Guimera, J.: ON matrix diffusion: formulations, solution methods and qualitative methods, Hydrogeol. J., 6, 178–190, 1998. 2444
Danckwerts, P. V.: Continous flow systems; distribution of residence times, Chem. Eng. Sci., 2, 2–3, 1953. 2443
de Hoog, F. R., Knight, J. H., and Stokes, A. N.: An improved method for numerical inversion of Laplace transforms, S.I.A.M. J. Sci. Stat. Comput., 3, 357–366, 1982. 2444
Fretwell, B. A., Burgessa, W. G., Barker, J. A., and Jefferies, N. L.: Redistribution of contaminants by a fluctuating water table in a micro-porous, double-porosity aquifer: Field observations and model simulations, J. Cont. Hydrol., 78, 27–52, 2005. 2444
Haggerty, R. and Gorelick, S. M.: Multiple-rate mass transfer for modeling diffusion and surface reactions in media with pore-scale heterogeneity, Water Resour. Res., 31, 2383–2400, 1995. 2449
Haggerty, R., McKenna, S. A., and Miggs, L. C.: On the late-time behaviour of tracer test breakthrough curves, Water Resour. Res., 36, 3467–3479, 2000. 2448, 2449
Haggerty, R., Fleming, S. W., McKenna, S. A., and Miggs, L. C.: Tracer tests in a fractured dolomite 2. Analysis of mass transfer in single-well injection-withdrawal tests, Water Resour. Res., 37, 1129–1142, 2001. 2449
Kachi, S.: Tracer studies in the Chalk aquifer near Cambridge, MPhil Thesis, University of East Anglia, Norwich, 1987. 2439, 2441
Lagarias, J. C., Reeds, J. A., Wright, M. H., and Wright, P. E.: Convergence Properties of the Nelder-Mead Simplex Method in Low Dimensions, SIAM J. Optim., 9, 112–147, 1998. 2450
Maloszewski, P. and Zuber, A.: On the theory of tracer experiments in fissured rocks with a porous matrix, J Hydrol., 79, 333–358, 1985. 2445
Mathias, S. A., Butler, A. P., McIntyre, N., and Wheater, H. S.: The sigificance of flow in the

matrix in the Chalk unsaturated zone, J. Hydrol, 310, 62–77, 2005. 2445
Mcintyre, N., Wheater, H., and Lees, M.: Estimation and propogtaion of parametric uncertainty in environmental models, J. Hydroinf., 4, 177–197, 2002. 2440
McKenna, S. A., Meigs, L. C., and Haggerty, R.: Tracer tests in a fractured dolomite 3. Double-porosity, multiple-rate mass transfer processes in convergent flow tracer tests, Water Resour. Res., 37, 1143–1154, 2001. 2440, 2449
Moench, A. F.: Convergent radial dispersion: A Laplace transform solution for aquifer tracer testing, Water Resour. Res., 25, 439–447, 1989. 2444
Moench, A. F.: Convergent radial dispersion in a double porosity aquifer with fracture skin: analytical solution and application to a field experiment in fractured Chalk, Water Resour. Res., 31, 1823–1835, 1995. 2439, 2440, 2442, 2443, 2444
Price, M., Downing, R. A., and Edmunds, W. M.: The Chalk as an aquifer, in: The Hydrogeology of the Chalk of North-West Europe, edited by: Downing, R. A., Price, M., and Jones, G. P., 35–58, Clarendon Press, Oxford, 1993. 2439
Schwartz, R. C., McInnes, K. J., Juo, A. S. R., and Wilding, L. P.: Boundary effects on solute transport in finite soil columns, Water Resour. Res., 35, 671–381, 1999. 2443
Sincock, A. M., Wheater, H. S., and Whitehead, P. G.: Calibration and sensitivity analysis of a river water quality model under unsteady flow conditions, J. Hydrol., 277, 214–229, 2003. 2440
Smith, R. M. S. and Wheater, H. S.: Multiple objective evaluation of a simple phosphorous transfer model, Hydrol. Proc., 18, 1703–1720, 2004. 2440
Wagener, T., Boyle, D. P., Lees, M. J., Wheater, H. S., Gupta, H. V., and Sorooshian, S.: A framework for development and application of hydrological models, Hydrol. Earth Syst. Sci., 5, 13–26, 2001. 2440
Ward, R.: Artificial tracer and natural ^{222}Rn studies of the East Anglian Chalk aquifer, Ph.D. thesis, University of East Anglia, Norwich, 1989. 2439, 2441
Ward, R.: Banterwick Barn tracer test. Data report, Technical Report WE/96/X, British Geological Survey, 1996. 2439
Ward, R., Williams, A. T., Barker, J. A., Brewerton, L. J., and Gale, I. N.: Groundwater Tracer Tests: a review and guidelines for their use in British aquifers, R&D Technical Report W160, Environment Agency, 1998. 2441
Wright, T. E.: Predicting the applicability of Aquifer Storage Recovery (ASR) to UK, Ph.D. thesis, University College London, 2002. 2450

Table 1. Summary of test details.

Test name	Horseheath	South Farm
County	Cambridgeshire	Norfolk
Tracer	Fluorescein	Flourescein
Quantity, M_{inj}	0.5 kg	0.5 kg
Abstraction rate, Q	2610 m^3/day	3326 m^3/day
Distance from pumped well, R	44 m	199 m
Aquifer	Middle Chalk	Upper Chalk

Table 2. Optimum parameter sets for the Horseheath tracer test.

Model	t_a (h)	t_{cf} (h)	t_{cb} (h)	P (–)	Mass recovery	RMSE (ppb)
PFDM	5.26	1.33	214	25.7	85%	4.79
SFDM	4.69	0.85	N/A	28.2	94%	5.54
DM	26.8	N/A	N/A	1.45	74%	10.9
PFM	2.07	0.14	421	N/A	95%	6.00
SFM	2.11	0.14	N/A	N/A	97%	6.16

Table 3. Optimum parameter sets for the South Farm tracer test.

Model	t_a (h)	t_{cf} (h)	t_{cb} (h)	P (–)	Mass recovery	RMSE (ppb)
PFDM	37.84	4.00	2058	53.6	54%	0.28
SFDM	37.84	4.00	N/A	53.6	54%	0.28
DM	219.5	N/A	N/A	3.04	31%	0.40
PFM	22.54	1.30	3021	N/A	56%	0.26
SFM	22.54	1.30	N/A	N/A	56%	0.26

Table 4. Calculated fracture spacings (i.e. $2b$) for a range of apparent diffusion coefficients (D_A) and characteristic block diffusion times ($t_{cb}=b^2/D_A$).

D_A (m^2/s)	10^{-10}	10^{-11}	10^{-12}
t_{cb} (hours)	Fracture spacing (m)		
10	3.8×10^{-3}	1.2×10^{-3}	3.8×10^{-4}
100	1.2×10^{-2}	3.8×10^{-3}	1.2×10^{-3}
1000	3.8×10^{-2}	1.2×10^{-2}	3.8×10^{-3}
10 000	1.2×10^{-1}	3.8×10^{-2}	1.2×10^{-2}

Table 5. Optimum SFDM parameter sets for the Horseheath tracer test assuming various values of P.

P (–)	t_a (h)	t_{cf} (h)	Mass recovery	RMSE (ppb)
∞	2.09	0.14	97%	6.16
100	2.92	0.29	96%	5.81
90	3.00	0.31	96%	5.78
80	3.11	0.33	96%	5.75
70	3.24	0.36	96%	5.71
60	3.41	0.41	96%	5.67
50	3.65	0.47	95%	5.62
40	3.98	0.58	95%	5.57
30	4.50	0.76	95%	5.53
20	5.44	1.19	94%	5.55
10	7.89	2.85	93%	5.86

Table 6. Optimum SFDM parameter sets for the South Farm tracer test assuming various values of P.

P (–)	t_a (h)	t_{cf} (h)	Mass recovery	RMSE (ppb)
∞	21.95	1.23	56%	0.26
100	30.07	2.41	55%	0.27
90	30.97	2.57	55%	0.27
80	32.08	2.77	55%	0.27
70	33.51	3.05	55%	0.27
60	35.40	3.44	55%	0.27
50	38.02	4.03	54%	0.28
40	41.88	5.00	54%	0.28
30	48.18	6.87	54%	0.29
20	60.29	11.6	52%	0.30
10	93.75	36.3	49%	0.32

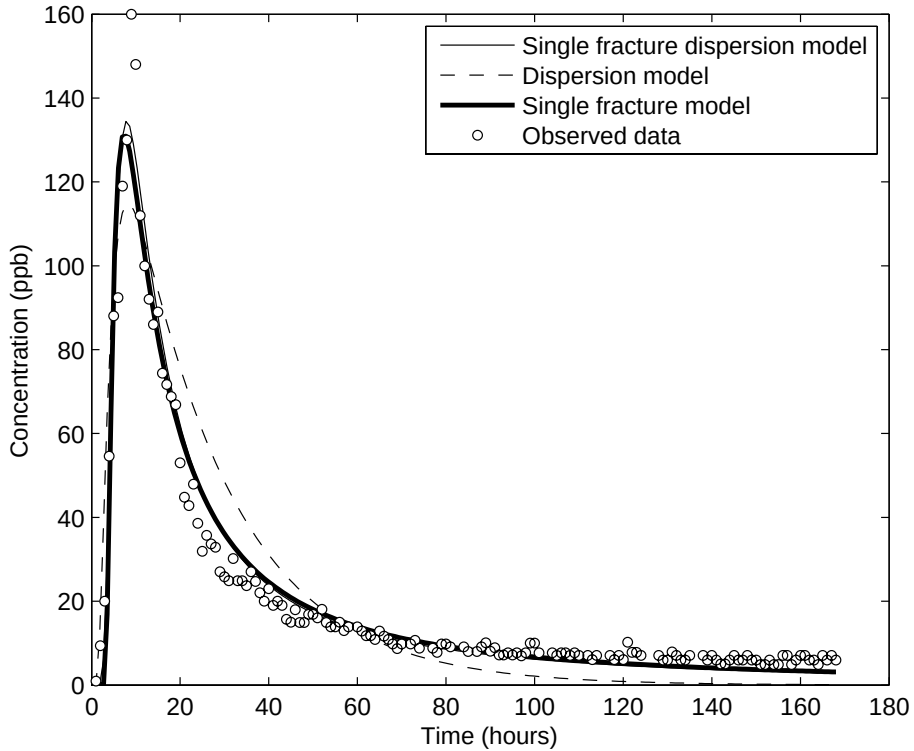

Fig. 1. Comparison of modelled and observed data for the Horseheath tracer test. For clarity the PFDM and PFM were omitted due to their similarity with the SFDM and SFM breakthrough curves.

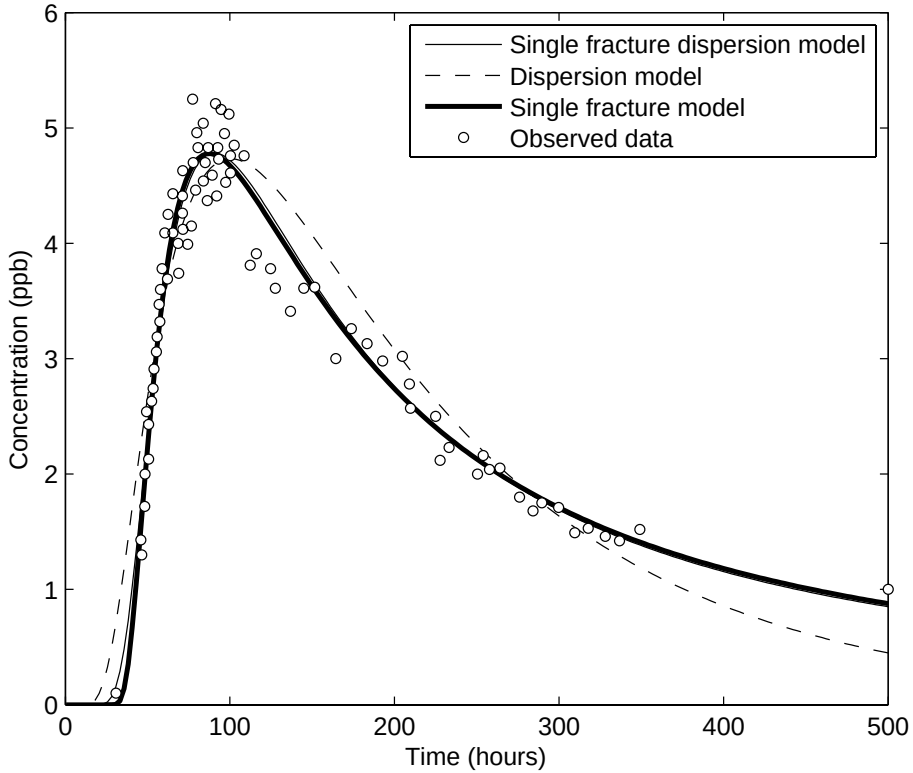

Fig. 2. Comparison of modelled and observed data for the South Farm tracer test. For clarity the PFDM and PFM were omitted due to their similarity with the SFDM and SFM breakthrough curves.

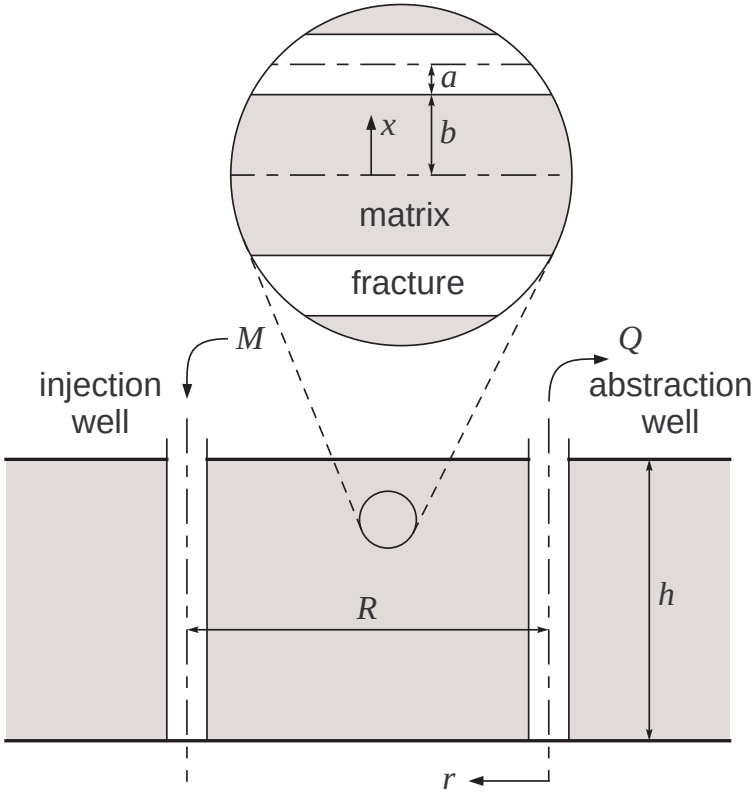

Fig. 3. Schematic diagram of model domain.

HESSD
3, 2437–2471, 2006

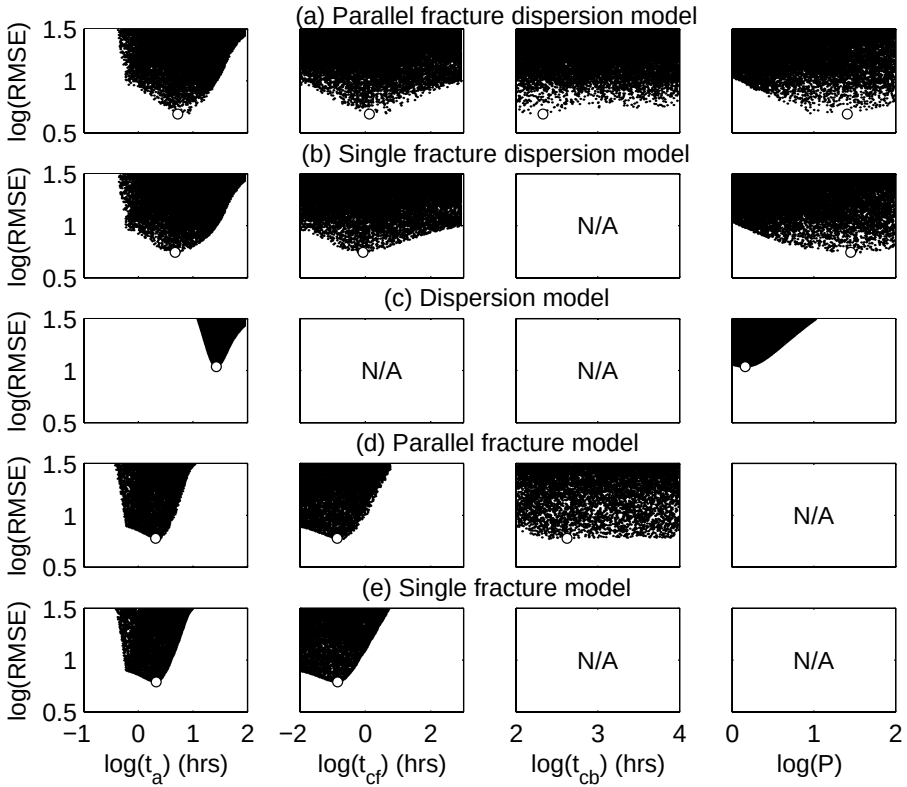

Fig. 4. Dotty plots from Monte Carlo simulations of the five models for the Horseheath tracer test. The limits on the x-axes are the upper and lower bounds of the a priori log-uniform random parameter distributions. Parameter sets with the lowest RMSE are marked with the "o" marker.

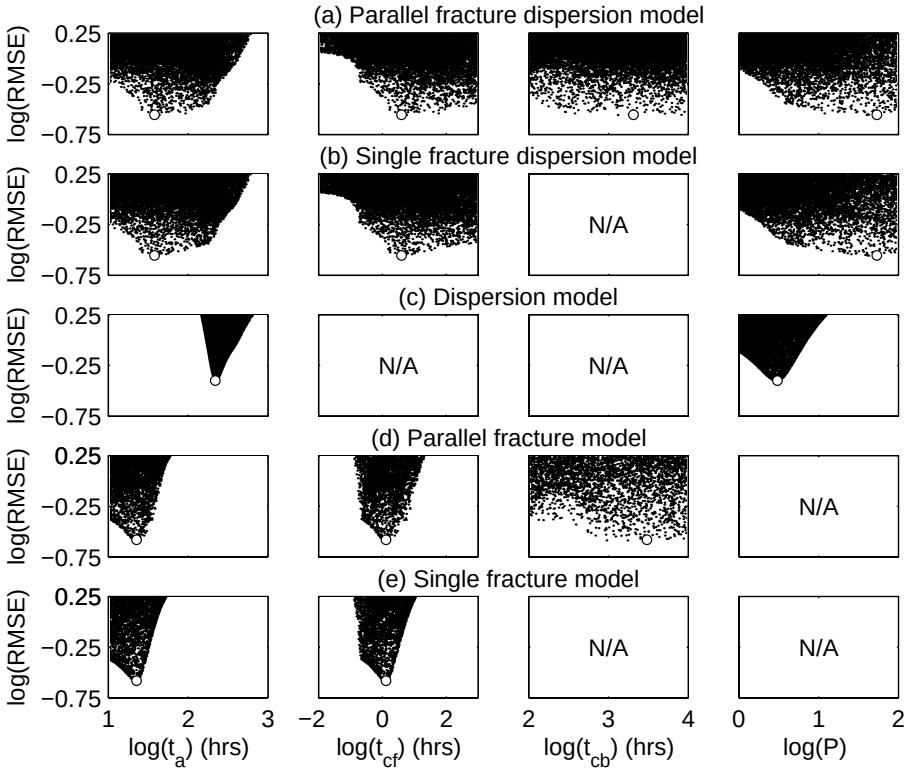

Fig. 5. Same as Fig. 3 but for the South Farm tracer test.

HESSD
3, 2437–2471, 2006

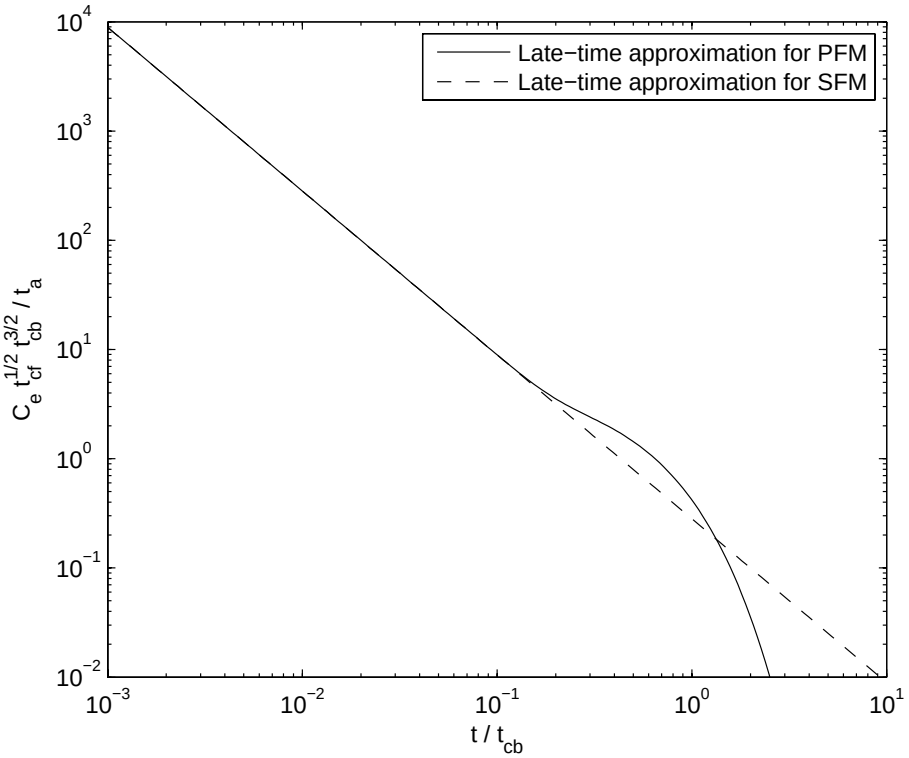

Fig. 6. The late-time breakthrough curves for both the PFM (Eq. 23) and the SFM (Eq. 24).

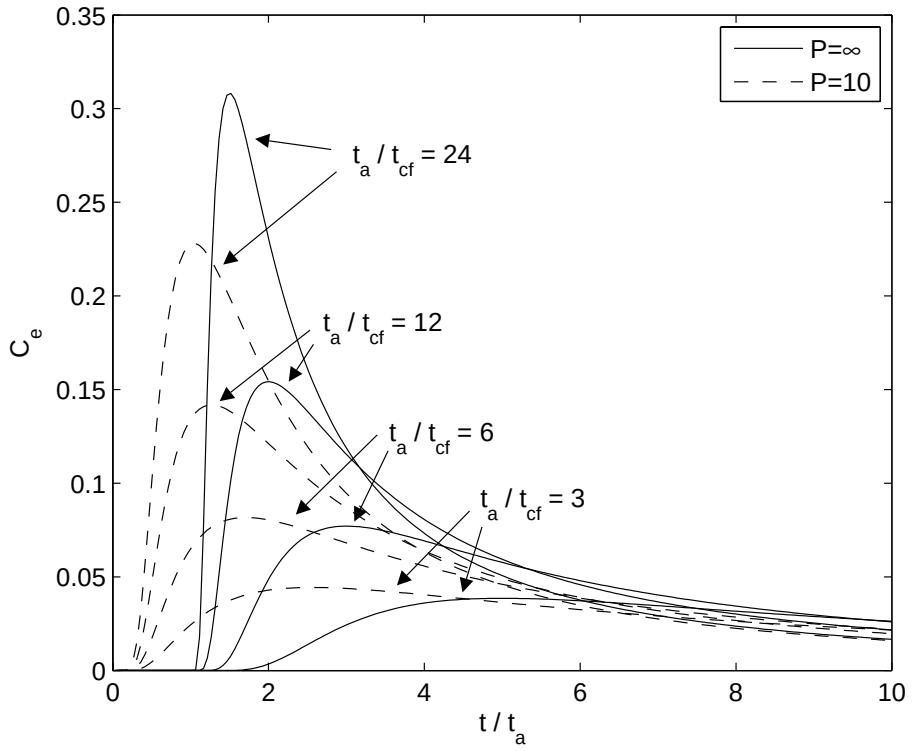

Fig. 7. Sensitivity plot comparing the SFM (i.e. $P=\infty$) with an equivalent (radially convergent) SFDM with $P=10$ for a range of t_a/t_{cf} ratios.

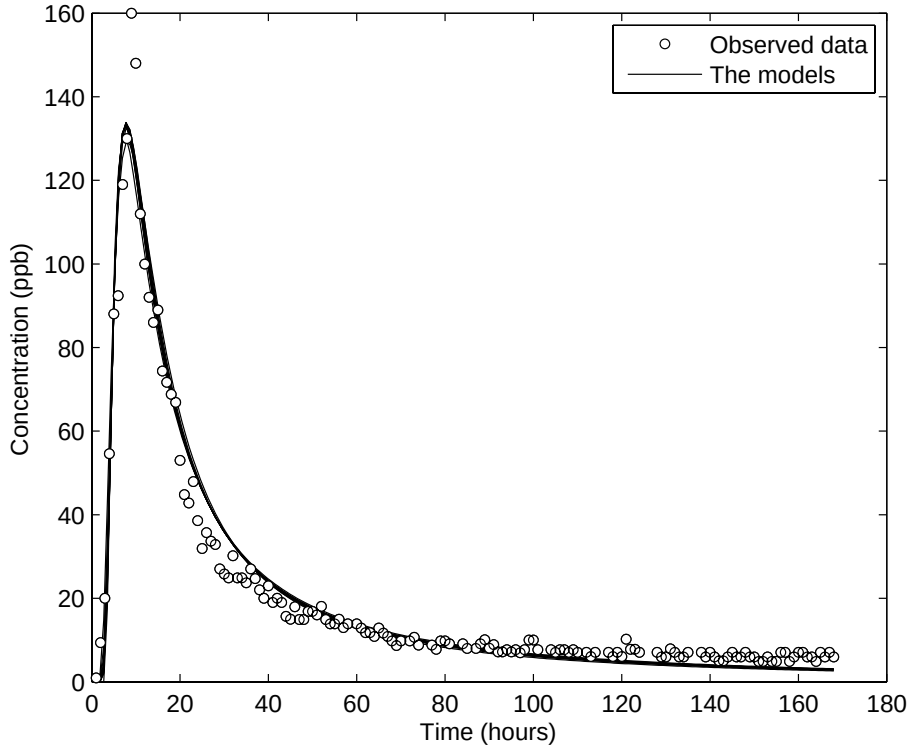

Fig. 8. Comparison of all the models detailed in Table 5 and the observed data for the Horseheath tracer test (plotted on linear scales).

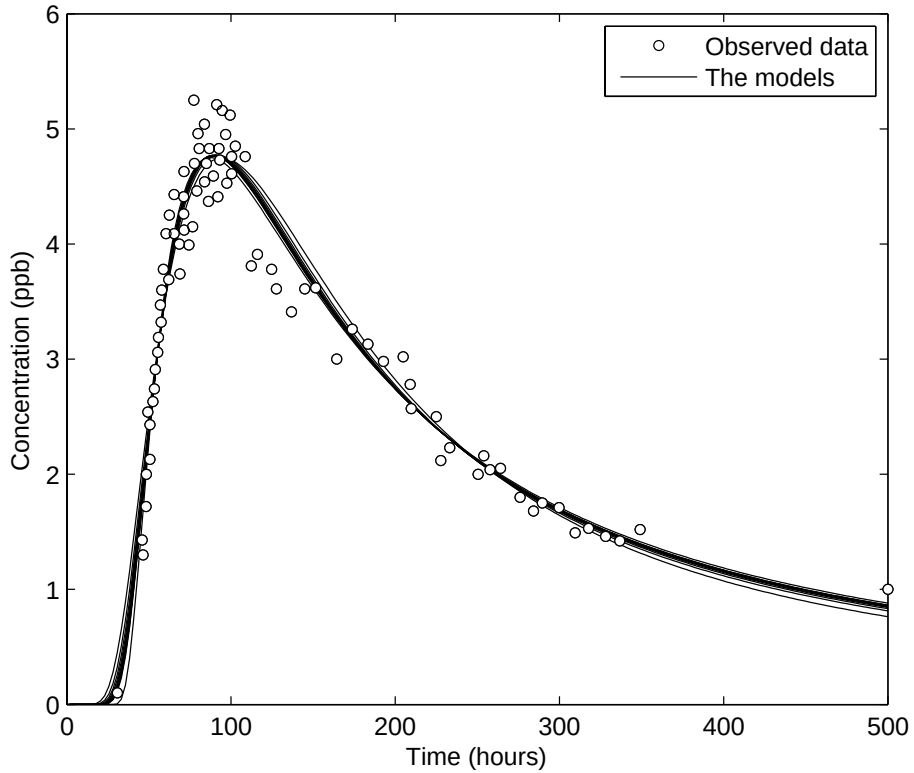

Fig. 9. Comparison of all the models detailed in Table 6 and the observed data for the South Farm tracer test (plotted on linear scales).

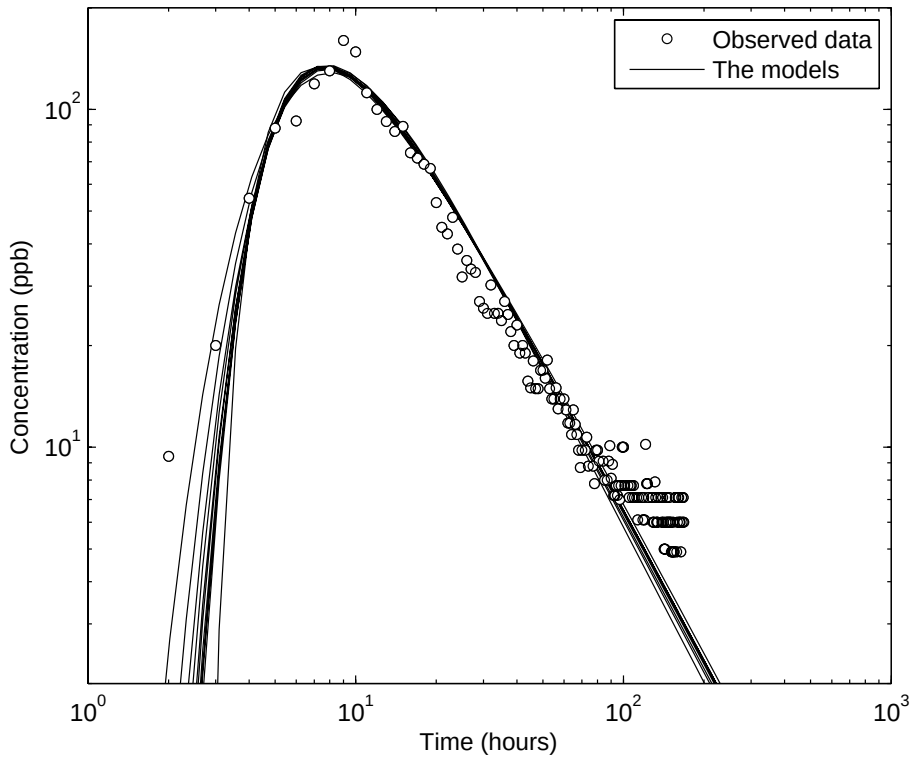

Fig. 10. Comparison of all the models detailed in Table 5 and the observed data for the Horseheath tracer test (plotted on log scales).

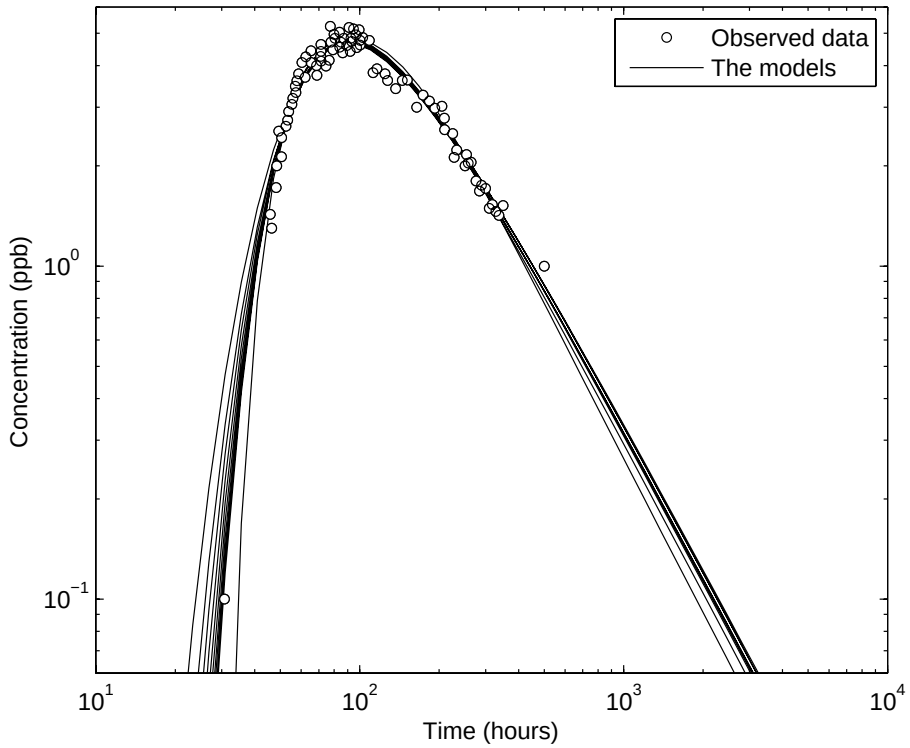

Fig. 11. Comparison of all the models detailed in Table 6 and the observed data for the South Farm tracer test (plotted on log scales).